Proceedings of Global Power and Propulsion Society
ISSN-Nr: 2504-4400
GPPS Xi'an21
18th–20th October, 2021

www.gpps.global

GPPS-TC-2021-0042

FLUTTER ANALYSIS OF BLISKS WITH FRICTION RING DAMPERS

Yekai Sun[a*] **Jie Yuan**[ab†] **Loïc Salles**[a‡]

a **Department of Mechanical Engineering, Imperial College London, London, SW7 2AZ, UK**

b **Aerospace Centre of Excellence, University of Strathclyde, Glasgow, G1 1XQ, UK**

E-mail: * ys5113@imperial.ac.uk; † jie.yuan@strath.ac.uk; ‡ l.salles@imperial.ac.uk

ABSTRACT

Aeroelastic flutter is a phenomenon when blades experience an aeroelastic self-excitation from the surrounding air resulting in the full destruction of aero-engines. It poses a big challenge for aero-engine bladed-disks design, especially for integrally bladed-disks (blisks). The lack of friction interfaces in blisks drastically reduces structural damping making them more likely to experience aeroelastic flutter. One of the most effective approaches to improve the damping in a blisk is the use of friction ring dampers. This paper presents a numerical study to investigate the effects of friction ring dampers on the aeroelastic stability of blisks. A lumped parameter model is used to represent the blisk with a ring damper. Aeroelastic self-excitations are simply represented by Van der Pol oscillators. The frictional contact between the blisk and ring damper is modelled by using Jenkins elements. Nonlinear modal analysis is used to compute the nonlinear dynamic response of the system. The results show that the friction ring damper can significantly reduce the risk of flutter and the amplitude of flutter induced limit cycle oscillations for a blisk by increasing the structural damping, especially at a high modal amplitude. The study also shows that the nonlinear modal analysis can efficiently identify the flutter boundary of such a strongly dissipated nonlinear system.

INTRODUCTION

In industrial turbomachinery, vibration is considered as a major cause for high cycle fatigue failures in bladed disks. The type of blade vibrations can be mainly classified into two groups: synchronous forced response and aeroelastic flutter. Flutter is a phenomenon of unstable aeroelastic interaction between bladed disks and their surrounding airflow, also known as aeroelastic self-excitation. In the case of flutter, because of the overall negative damping in the system, the energy is injected into bladed disks from the surrounding airflow. When flutter occurs, the amplitude of blade vibration grows unrestrainedly until the structure fails as the negative aerodynamic damping will continuously inject the energy into the system. If the structural damping can completely balance the negative aerodynamic damping, the flutter induced Limit Cycle Oscillation (LCO) can be seen. Flutter in bladed disks has been investigated in the field of fluid dynamics by several researchers Zhao et al. (2017); Vahdati et al. (2011); Stapelfeldt and Brandstetter (2020). In Salles and Vahdati (2016), two numerical algorithms for computing the effects of fan flutter were compared in detail. To avoid catastrophic failures due to the flutter, various frictional damping techniques have been attempted to introduce structural damping to avoid the occurrence of flutter or reducing the amplitude of flutter induced LCO. The traditional bladed disks consist of several blades and a disk. There are many contact interfaces within the assembly. Whereas for blisks, also known as integrally bladed disks, since they are manufactured by a single piece of material, there is no contact interface in the system which makes the structural damping much lower than bladed disks. Therefore, to improve the damping performance of the blisk, friction ring dampers (FRDs) are recently introduced to provide additional friction interfaces. Essentially, a FRD is a ring-type structure located within the groove underneath the disk. The nonlinear dynamics of a blisk with FRD has been investigated by several researchers Laxalde et al. (2008, 2010); Sun, Yuan, Denimal and Salles (2021); Tang and Epureanu (2019); Lupini and Epureanu (2020); Wu et al. (2020).

In the actual design of blisks, if the vibrations of blisks are excited through an aeroelastic self-excited mechanism, the aerodynamic damping of the system is negative. In this case, the design of FRDs is necessary to compensate the negative aerodynamic damping. The aerodynamic force for a full-scale structure can be obtained from the direct computation of fluid dynamics with a considerable computational burden. In a low fidelity simulation, aeroelastic self-excitations are simplified by Van der Pol (VdP) oscillators Dowell (1981); Facchinetti et al. (2004). One of the advantages of using VdP oscillators is the conversion of negative damping into a positive one after the amplitude exceeds critical limits. VdP oscillator is a

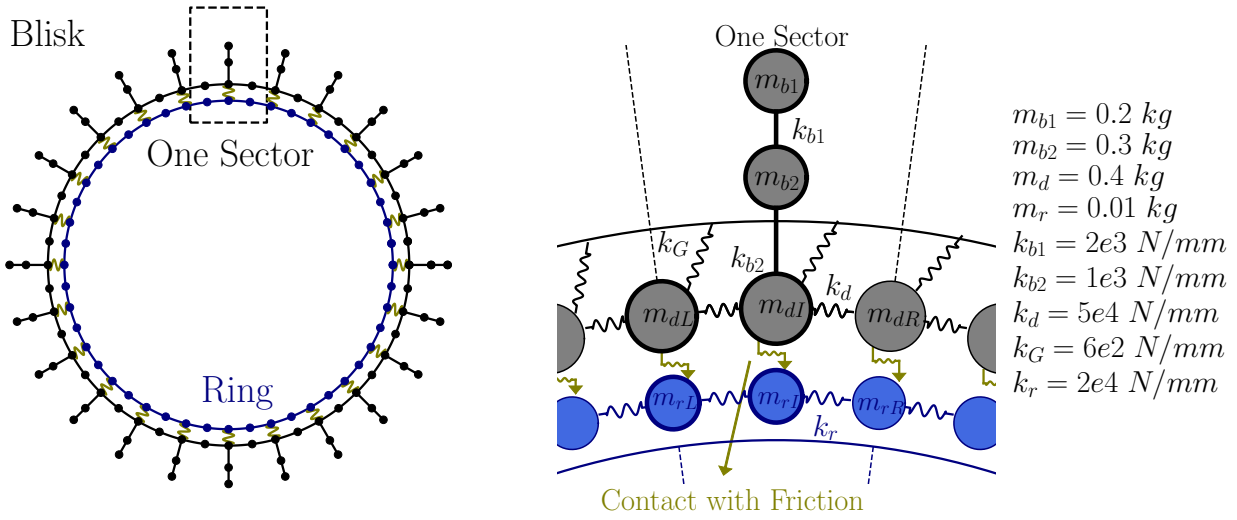

Figure 1 Lumped parameter model for blisk with ring damper: full annulus and an elementary sector

suitable representation for the aeroelastic self-excitation for a phenomenological simulation using illustrative models Půst et al. (2018); Půst and Pešek (2017); Pešek et al. (2019). Due to the presence of frictional contact and VdP oscillators, the dynamic response of such an aeroelastic system is strongly nonlinear and complicated. The classic methods for linear dynamics are not suitable anymore and advanced methods for nonlinear dynamic analysis are needed.

Nonlinear Normal Modes (NNMs) can be used to study the nonlinear dynamic responses. Compared to linear systems, the orthogonality and superposition of the linear modes are not valid for NNMs. The periodic definition of NNMs was firstly proposed in Rosenberg (1960), as a family of periodic solutions. Then, the NNMs were geometrically defined as an invariant manifold in Shaw and Pierre (1991), which extended the definition of NNMs to nonlinear non-conservative systems. The NNMs in non-conservative systems are named as damped Nonlinear Normal Modes (dNNMs) Sarrouy (2019); Sun, Yuan, Vizzaccaro and Salles (2021), which are typically non-periodic (decaying or growing in the time history). To extended the periodic definition of NNMs to dNNMs, two concepts were proposed in the last two decades, complex nonlinear mode by Laxalde and Thouverez (2009) and Extended Periodic Motion Concept (EPMC) by Krack (2015). In EPMC, dNNMs were formulated in a periodic form by introducing artificial damping into such systems to compensate the energy exchanged by the non-conservative nonlinear forces (i.e. VdP oscillator or frictional contact). Thanks to EPMC, dNNMs can be directly represented as harmonic solutions and classic numerical methods for periodic problems (i.e. Harmonic Balance Method (HBM) Urabe (1965)) can be simply implemented. Furthermore, the use of dNNMs has also been proved to be an efficient method to predict the self-excited solutions in the case of friction-induced vibration in Sun, Vizzaccaro, Yuan and Salles (2021). To the best of the authors' knowledge, using nonlinear modal analysis to investigate the aeroelastic flutter phenomena for blisks has never been attempted in the literature.

This work aims to propose a modelling strategy to investigate the effects of friction damping on aeroelastic stability for a blisk with a friction ring damper. In this study, aerodynamic excitation is simplified by a VdP nonlinear oscillator. EPMC based nonlinear modal analysis is then used to compute the self-excitation solutions. This paper is organised as follows: the Lumped Parameter Model (LPM) to represent the blisk and FRD will be introduced at first; it is followed by the description of VdP oscillator and frictional contact model; then, the formulations to obtain dNNMs are presented; after that, results of flutter region and flutter induced LCOs are demonstrated using dNNMs and discussed followed by the conclusions.

MODEL DESCRIPTION

Blisk and Ring Damper

A LPM is used in this work to represent the full scale of blisk with FRD. This LPM (see Fig.1) has been used in the existing research Laxalde et al. (2007); Sun et al. (2018). There are total eight Degree of Freedoms (DoFs) per sector, which are used to represent the blisk: two DoFs for the blade ($\underline{q}_{b1}$ and $\underline{q}_{b2}$), three DoFs for the disk (internal $\underline{q}_{dI}$, right $\underline{q}_{dR}$ and left $\underline{q}_{dL}$) and the other three for the FRD (internal $\underline{q}_{rI}$, right $\underline{q}_{rR}$ and left $\underline{q}_{rL}$). There are 24 sectors in total within this cyclic symmetric structure, $N_s = 24$. The model parameters are listed in Fig.1. The blisk and FRD are assumed to be identical among each sector. The Mead's approach Mead (1975) is used to apply cyclic boundary conditions. After applying the cyclic symmetric boundaries, the DoFs associated with the right boundaries (q_{dR} and q_{rR}) are eliminated. The DoFs retained after the cyclic symmetric reduction are: $\underline{Q} = [\underline{q}_{b1}, \underline{q}_{b2}, \underline{q}_{dI}, \underline{q}_{dL}, \underline{q}_{rI}, \underline{q}_{rL}]^{\mathrm{T}}$.

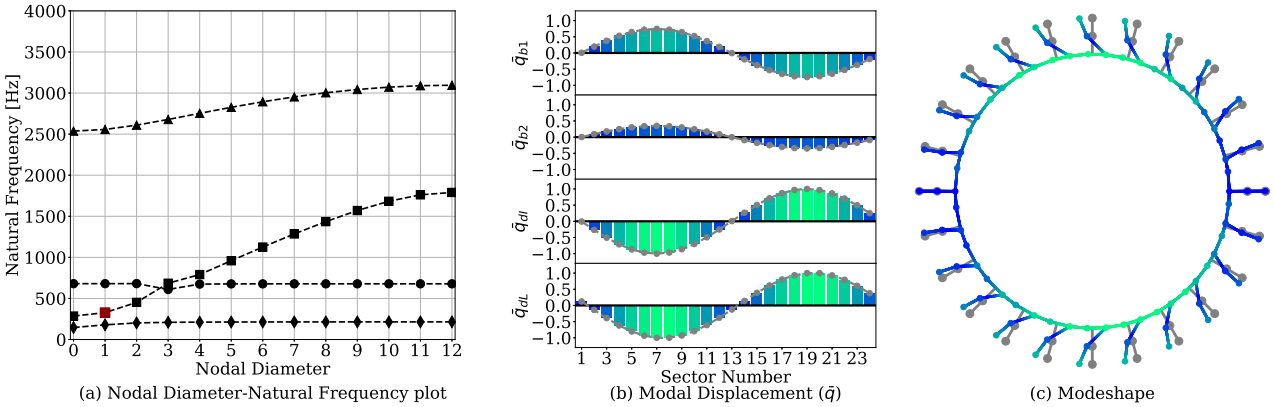

(a) Nodal Diameter-Natural Frequency plot (b) Modal Displacement ($\bar{q}$) (c) Modeshape

Figure 2 Natural frequency against nodal diameter and mode shape for the third modal family with nodal diameter 1

Linear modal analysis

The natural frequencies of the LPM (without the FRD) are plotted against the Nodal Diameter (ND) in Fig.2(a). There are four families of modes, two of them blade dominated modes (diamonds and circles). The natural frequencies of these two families are almost constant for all possible NDs. Whereas, the other two (squares and triangles) are disk dominated modes. For disk dominated modes, the modal stiffness increases dramatically with a growing ND because of the blade-disk coupling effect. The blade-disk coupling effect gives access for communication of the vibration energy between blades and disks. The FRDs are designed to reduce the vibration amplitude for the mode with a large disk displacement. Therefore, the modes from 3^{rd} modal family (represented by squares) are selected for the following study. The mode shape of 3^{rd} modal family with ND 1 is shown in Fig.2(b, c). By looking at the mode shape, the DoFs associated with the disk show a significant modal displacement.

Equation of Motion

The general Equation of Motion (EoM) for nonlinear modal analysis is given in Eqn.(1), where $\underline{\underline{\mathbf{M}}}$ and $\underline{\underline{\mathbf{K}}}$ are the mass and stiffness matrices. In nonlinear modal analysis, the linear damping is usually not considered. $\underline{Q}(t)$ is the periodic solutions of the present EoM, the underline of the symbol is used to represent the vector and variable t does not appear explicitly in the following equations. $\underline{F}_f(\underline{Q},\dot{\underline{Q}})$ is the friction force between the blisk and FRD; $\underline{F}_a(\underline{Q},\dot{\underline{Q}})$ is the aeroelastic self-excitation applied to the blade.

$$\underline{\underline{\mathbf{M}}}\,\ddot{\underline{Q}}(t)+\underline{\underline{\mathbf{K}}}\,\underline{Q}(t)+\underline{F}_f(\underline{Q},\dot{\underline{Q}})+\underline{F}_a(\underline{Q},\dot{\underline{Q}})=0 \tag{1}$$

Modelling aeroelastic self-excitation

The aerodynamic excitation is represented by the classic VdP oscillator. In a VdP oscillator, the aerodynamic damping is negative, and it increases with the vibration amplitude. One of the great advantages of this model is that positive damping can be achieved when the amplitude of self-excitation exceeds a prescribed limit Půst et al. (2018). There are two critical parameters within the VdP oscillator, which are β_1 and β_2. These two critical parameters are expected to be tunned using empirical aerodynamic data. The aerodynamic excitation is assumed to be applied on the blade DoF 1 $\underline{q}_{b1}$. The values of β_1 and β_2 are selected by the authors to demonstrate the potential for such a model.

$$\underline{F}_a=-\beta_1\cdot\dot{\underline{q}}_{b1}+\beta_2\cdot\underline{q}_{b1}^2\dot{\underline{q}}_{b1} \tag{2}$$

Modelling friction

The frictional contact between the blisk and FRD is modelled by a 1D contact element Jenkins (1962). This 1D contact element consists of a Jenkins element in tangential direction with a constant normal load as shown in Fig.3(a). N_0 is the constant normal load 500 N; k_t is the tangential contact stiffness $5e6\ N/m$; μ is the friction coefficient 0.5. $x(t)$ is periodic tangential relative displacement between the contact pairs; $w(t)$ is the relative displacement of the contact point. For a current time step i, relative displacement $x(t_i)$, the displacement of the contact point $w(t_i)$ and the friction force $F_x(t_i)$ are calculated iteratively. The tangential friction forces is predicted using $f_{pre}=k_t(x(t_i)-w(t_{i-1}))$, then corrected in Eqn.(3). The relative displacement can be calculated by $x(t)=q_{dI}(t)-q_{rI}(t)$ or $x(t)=q_{dL}(t)-q_{rL}(t)$. After applying Eqn.(3), the friction force can be computed and shown in Fig.3(b, c, d).

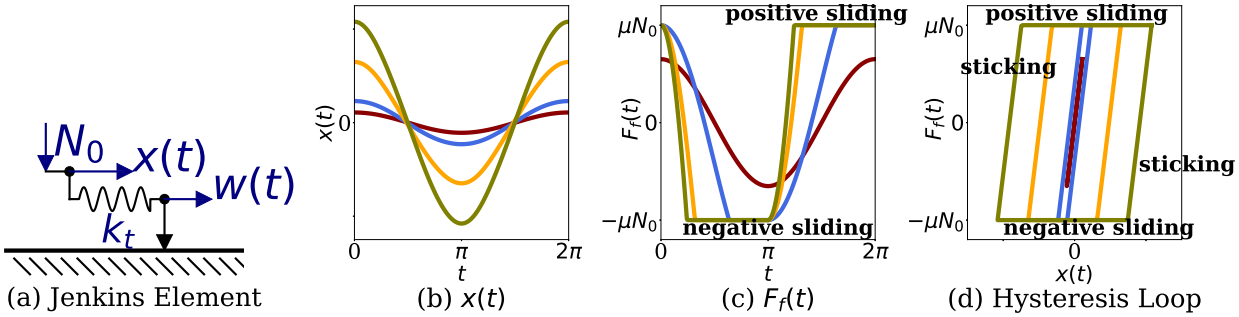

(a) Jenkins Element (b) $x(t)$ (c) $F_f(t)$ (d) Hysteresis Loop

Figure 3 Contact element: (a) Jenkins element; (b) Relative displacemet; (c) Friction force; (d) Hysteresis loops

$$\begin{cases} \text{if} \quad f_{pre} < \mu N_0 \quad \text{Sticking:} & F_f(t_i) = f_{pre} & w(t_i) = w(t_{i-1}) \\ \text{if} \quad f_{pre} \geq \mu N_0 \quad \text{Sliding:} & F_f(t_i) = \mu N_0 \cdot f_{pre} / \left| f_{pre} \right| & w(t_i) = x(t_i) - F_f(t_i)/k_t \end{cases} \tag{3}$$

COMPUTATION OF DAMPED NONLINEAR NORMAL MODE

The dNNMs are not in a periodic form because of the non-conservative nonlinear forces. The dNNMs are computed based on EPMC, which was proposed by Krack (2015). The basic idea of EPMC is that using an artificial viscous damping term to balance the energy exchanged by the non-conservative nonlinearities. Thanks to the artificial damping, the dNNMs can be represented using harmonic formulations and the classic HBM method can be applied. The modal damping ratio ζ of this artificial damping term is defined as ζ, which is considered as a free parameter and expected to be determined in the computation of dNNMs. This modal damping ratio ζ is used to quantify the amount of energy exchanged. For example, in the system with frictional contact, the total energy is dissipated leading to a positive modal damping ratio. Whereas in the case of a self-excited system, a negative modal damping ratio can be seen. After the introduction of this artificial negative damping term, the EoM is rewritten as Eqn.(4), where ω_0 is the resonant frequency of the dNNM. $2\zeta\omega_0\underline{\underline{\mathbf{M}}}\,\dot{\underline{Q}}$ is the artificial viscous damping term.

$$\underline{\underline{\mathbf{M}}}\,\ddot{\underline{Q}}(t) + \underline{\underline{\mathbf{K}}}\,\underline{Q}(t) - 2\zeta\omega_0\underline{\underline{\mathbf{M}}}\,\dot{\underline{Q}} + \underline{F}_f(\underline{Q},\dot{\underline{Q}}) + \underline{F}_a(\underline{Q},\dot{\underline{Q}}) = \underline{0} \tag{4}$$

Harmonic Balance Method

The classic HBM is applied to solve Eqn.(4) in the frequency domain Cameron and Griffin (1989). In the framework of HBM, the solutions $\underline{Q}$, the nonlinear forces $\underline{F}_f$ and $\underline{F}_a$ are represented by series of harmonic functions with the resonant frequency ω_0. The periodic solutions and forces are decomposed by the Fourier series truncated up to N_h order of harmonics, as shown in Eqn.(5). $\tilde{\underline{Q}}_n$ is the complex Fourier coefficient for the n^{th} order of harmonics. j represents the imaginary parts.

$$\underline{Q}(t) = \Re\{\sum_{n=0}^{N_h} \tilde{\underline{Q}}_n e^{j\cdot n\omega_0 t}\};\ \tilde{\underline{Q}}_n = \tilde{\underline{Q}}_n^c - j\tilde{\underline{Q}}_n^s \tag{5}$$

Substituting Eqn.(5) into Eqn.(4) and balancing the harmonic terms with a Galerkin projection. Then, this EoM in time domain is transformed into the frequency domain, where $\tilde{\underline{Q}}$ is a collection of Fourier coefficients: $\tilde{\underline{Q}} = [\tilde{\underline{Q}}_0, \tilde{\underline{Q}}_1, \cdots, \tilde{\underline{Q}}_{N_h}]^{\mathrm{T}}$. $\tilde{\underline{F}}_f$ and $\tilde{\underline{F}}_a$ have the similar form with $\tilde{\underline{Q}}$. The EoM in frequency domain is provided in Eqn.(6-7). Furthermore, it is difficult to directly calculate the friction force in the frequency domain. Therefore, the classic alternating frequency/time method is applied to iteratively compute $\tilde{\underline{F}}_{f,}(\tilde{\underline{Q}})$, as described in Cameron and Griffin (1989).

$$\underline{\underline{\mathbf{Z}}}\,\tilde{\underline{Q}} + \tilde{\underline{F}}_{f,}(\tilde{\underline{Q}}) + \tilde{\underline{F}}_{a,}(\tilde{\underline{Q}}) = 0 \tag{6}$$

$$\underline{\underline{\mathbf{Z}}} = \mathrm{diag}(\underline{\underline{\mathbf{Z}}}_0, \underline{\underline{\mathbf{Z}}}_1, \ldots, \underline{\underline{\mathbf{Z}}}_{N_h});\quad \underline{\underline{\mathbf{Z}}}_n = -n^2\omega_0^2\underline{\underline{\mathbf{M}}}\,\tilde{\underline{Q}}_n - j2n\zeta\omega_0^2\underline{\underline{\mathbf{M}}}\,\tilde{\underline{Q}}_n + \underline{\underline{\mathbf{K}}}\,\tilde{\underline{Q}}_n \tag{7}$$

Unlike the linear modes, the dNNMs and other modal properties are highly energy-dependent. The modal displacement $\underline{Q}$, the resonant frequency ω_0 and the modal damping ratio ζ vary with the level of energy within the system. To capture this energy dependence, a new parameter, the modal amplitude α, is introduced into the system to quantify the modal energy. Then, the modal displacement can be expressed as: $\underline{Q} = \alpha \cdot \underline{Q}^0$, where $\underline{Q}^0$ is the mass normalised modal displacement. The mass normalised modal displacement is achieved by applying a mass normalisation constraint. In addition, the absolute phase of dNNMs is arbitrary. Therefore, a phase normalisation is required. Both constraints are applied in a similar way with Sun et al. (2020).

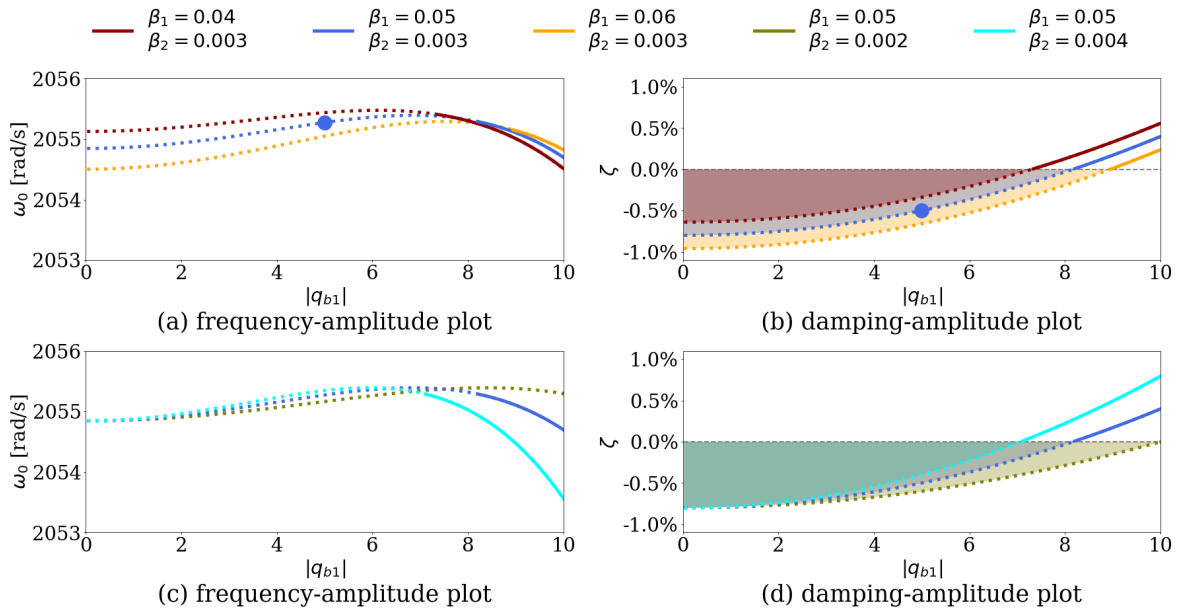

Figure 4 Damped nonlinear normal modes for Case A: (a, b) For different β_1; (c, d) For different β_2

Continuation method

The continuation method is a numerical method that can be used to track the evolution of a systematic behaviour against one or several of the system parameters. There are two major benefits of using continuation techniques. Firstly, the continuation technique is able to distinguish the solutions which are very close to each other. Secondly, they can be used to find different solutions for the same parameter. In a nonlinear case, more than one solution can coexist for one parameter. For nonlinear modal analysis, the modal amplitude is considered as the chasing parameter to track the evolution of the dNNM against the vibration amplitude. Readers are invited to refer Allgower and Georg (2003) for a detailed description.

RESULTS AND DISCUSSION

In the previous sections, the mechanical model and related numerical methodology for the present work are presented. In this section, we will show the result of this self-excited system from nonlinear modal analysis and related parametric studies. The dNNMs are used to represent the flutter induced LCOs of blisk with FRD under aeroelastic self-excitation. The effects of FRD and aeroelastic self-excitation on the resonant frequency ω_0 and modal damping ratio ζ of the dNNM will be discussed in detail. The present work consists of 3 scenarios. For Case A, the FRD is not included within the system and only the aeroelastic self-excitation based on VdP is considered. For Case B, the FRD is introduced into the system but it is assumed to be fully sticking. Finally, for Case C, the FRD involves both sticking and slipping states.

The results are shown in the form of frequency-amplitude ($\omega_0 - |q_{b1}|$) curves and the damping-amplitude ($\zeta - |q_{b1}|$) curves. The vibration amplitude is extracted from the first blade DoF $|q_{b1}|$. The part of the curve (where $\zeta < 0$, dotted part of the curves) represents the possible flutter induced LCOs depending on the material damping of the structure, and the region filled by colours in the figure is where the flutter can occur. Taking the blue point in Fig.4 (a, b) as an example, there exists a flutter induced LCO with an amplitude of 5 mm and a frequency of 2055.27 rad/s, if the material damping of the system equals $-\zeta$ (0.5%). If the material damping is smaller than $-\zeta$, the solutions of the system are unstable at an amplitude of 5 mm and a frequency of 2055.27 rad/s (vibration amplitude of the system will gradually grow). The flutter phenomenon can be seen.

Aeroelastic flutter of the blisk

The aeroelastic self-excitation is represented by the VdP oscillator, which has one negative linear damping and a positive nonlinear quadratic nonlinear term. β_1 controls the negative linear damping and β_2 represents the positive nonlinear quadratic damping. The values of these two parameters are selected by authors to show the potential of such a modelling strategy. In a real design situation, the aeroelastic self-excitation can be obtained from a direct computation of fluid dynamics. Here, the VdP oscillator is used to represent the given aeroelastic self-excitation for such a low fidelity simulation. The results are shown in Fig.4. Generally, one can notice that an increase in β_1 can lead to a lower ω_0 and a lower ζ at small amplitude. Whereas β_2 does not have significant effects on ω_0 and ζ at small amplitude but can affect the slopes of the $\zeta - |q_{b1}|$ curves.

From the Fig.4, it is obvious to obtain a general trend for the evolution of the ω_0 and ζ with respect to $|q_{b1}|$. At a

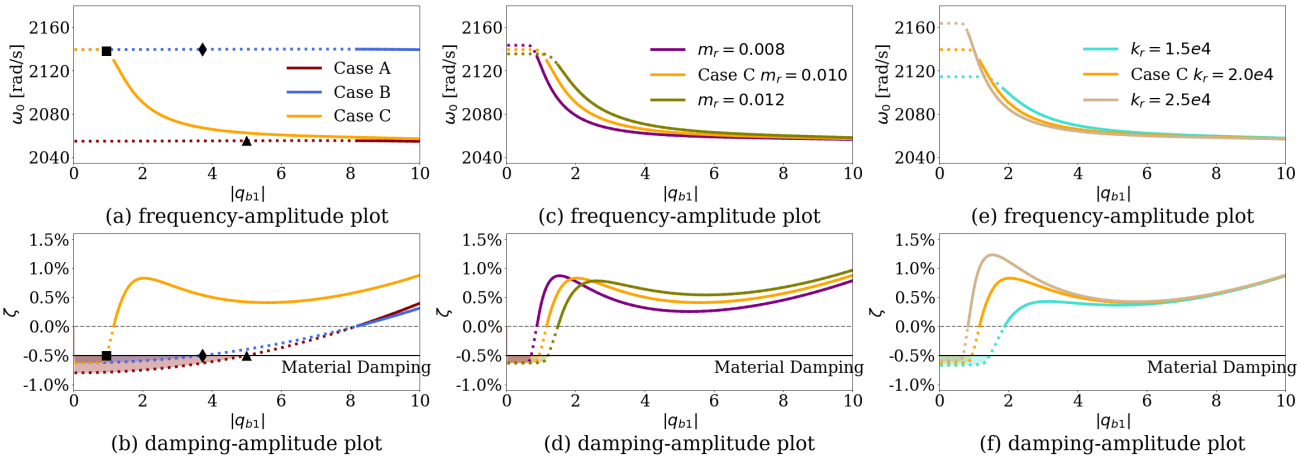

(a) frequency-amplitude plot (c) frequency-amplitude plot (e) frequency-amplitude plot

(b) damping-amplitude plot (d) damping-amplitude plot (f) damping-amplitude plot

Figure 5 Damped nonlinear normal modes: (a, b) For Case A, B and C; (c, d) For different m_r; (e, f) For different k_r

low level of $|q_{b1}|$, one can notice a negative ζ, which comes from the negative linear damping term. An increase in $|q_{b1}|$ leads to increase in ζ. Once the $|q_{b1}|$ exceeds the critical displacement. A positive ζ can be obtained. As for the change of the resonant frequency, when $\zeta < 0$, ω_0 increases from the natural frequency and starts to decrease when $\zeta > 0$. In the case of the blisk with flutter phenomenon, the surrounding airflow can impact the total mass, stiffness and damping of the system resulting in a resonant frequency that is different from the natural frequency of the blisk. However, the mass ratio between the surrounding airflow and the blisk is very small. Thus, the change in the frequency caused by the surrounding airflow usually can be ignored. From the Fig.4 (a, c), the variation of ω_0 is less than $\pm 0.2\%$, which provides a good physical representation of the real situation.

To further demonstrate the $\zeta - |q_{b1}|$ curves, we take the case of $\beta_1 = 0.05$, $\beta_2 = 0.003$ as an example. When the amplitude is less than 8.21 *mm*, the ζ is negative indicating that the system is physically unstable. It means that additional damping (i.e. material damping) is required to balance the negative damping introduced by the aeroelastic self-excitation to avoid the flutter. When the amplitude exceeds 8.21 *mm* (the solid part of the curves), the flutter induced LCOs cannot exist and the system is always stable.

Aeroelastic flutter of the blisk with ring damper

After the parametric study of the critical coefficients of the aeroelastic self-excitation, the values of β_1 and β_2 are selected as 0.05 and $= 0.003$ for the rest of the study. The $\omega_0 - |q_{b1}|$ curves and $\zeta - |q_{b1}|$ curves for Case B and Case C are shown and compared with Case A. Results are shown in Fig.5(a, b). It is worth reminding that Case B represents the blisk with a sticking FRD and aeroelastic self-excitation, whereas in Case C, the FRD can be both sticking and sliding.

For $\omega_0 - |q_{b1}|$ curves, it is obvious to notice that the effects from aeroelastic self-excitation are almost negligible. The evolution of ω_0 of Case C is a typical softening effect for structures with friction dampers Sun et al. (2020). At a low amplitude, the ring damper is sticking to the blisk, the $\omega_0 - q_{b1}$ curve for Case C is overlapped with the one of Case B. With an increasing amplitude, the ring starts to slide and the system is less stiff leading to a decreasing ω_0. Finally, the ω_0 of Case C will asymptotically tend to the ω_0 of Case A.

By looking at Fig.5(b), the ζ starts from -0.63% at zero amplitude. When $|q_{b1}|$ increases to 0.76 *mm*, the FRD starts to slide and dissipate the total energy of the system leading to a positive friction damping. The ζ dramatically increases and becomes positive at the amplitude of 1.16 *mm*. It is obvious to identify that, with the help of FRD, the flutter region is much smaller than that in Case A. In nonlinear modal analysis, material damping is not included in the computation of dNNMs. If the material damping is 0.5%, then flutter induced LCOs are highlighted by black markers. By comparing the amplitudes of these flutter induced LCOs, the one in Case C has the lowest amplitude.

Effects of the ring damper mass and stiffness

The results from the previous section has proven that FRDs can be seen as an efficient damping device to reduce the possibility of aeroelastic flutter and the amplitude of flutter induced LCOs of the blisk. Then, different values of the m_r ($m_r = 0.008\ kg$, the default case $m_r = 0.01\ kg$ and $m_r = 0.012\ kg$) and k_r ($k_r = 1.5e4\ N/mm$, the default case $k_r = 2e4\ N/mm$ and $k_r = 2.5e4\ N/mm$) are tested to further explore the possibility of the future design of FRDs. Results are provided in Fig.5(c, d, e, f).

In Fig.5(c, d), the $\omega_0 - |q_{b1}|$ curves and $\zeta - |q_{b1}|$ curves for three different values of m_r are shown. Changing the damper mass can directly influence the normal load N_0 and the inertia of the FRD. A lower value of m_r leads to a stiffer system and smaller flutter region. The maximum value of ζ does not change significantly. Whereas for the effects of k_r,

both ω_0 and ζ experience obvious influences. A higher k_r makes the system less flexible resulting in a greater ω_0. The flutter region can be also reduced by an increase in the stiffness of FRD.

CONCLUSIONS

This paper provides a numerical solution to the design of the friction ring dampers for blisks to investigate the flutter boundary in turbomachinery with a given aeroelastic self-excitation. A qualitative flutter analysis for blisks with friction ring damper is achieved using a lumped parameter model, Van der Pol oscillators and Jenkins elements. The phenomenological results are represented using the damped nonlinear normal modes to investigate the effects of the ring damper on the flutter boundary and flutter induced limit cycle oscillations. With the introduction of the ring damper, the possible flutter region of the studied mode and the amplitude of flutter induced limit cycle oscillations can be significantly reduced. Furthermore, a proper design of the friction ring damper can further improve the damping performance.

This work can be considered as the first attempt to use damped nonlinear normal modes to study the blisk with friction dampers under aeroelastic self-excitation. Using damped nonlinear normal modes is very straightforward to identify the flutter regions and flutter induced limit cycle oscillations. A full-scale structure and a more accurate representation of aeroelastic self-excitation will be considered in the near future.

ACKNOWLEDGMENTS

Dr Yekai Sun is grateful to China Scholarship Council (File NO. 201708060239) for providing the financial support for this project. Dr Jie Yuan acknowledges financial support from EPSRC (SYSDYMATS Project WP3). Dr Loïc Salles has received funding from Rolls-Royce and the EPSRC under the Prosperity Partnership Grant CornerStone (EP/R004951/1).

We thank Dr Fanzhou Zhao (Imperial College London, UK) for useful discussions.

REFERENCES

Allgower, E. L. and Georg, K. (2003), 'Introduction to Numerical Continuation Methods', *Classics in Applied Mathematics* **45**, xxvi–388.

Cameron, T. M. and Griffin, J. H. (1989), 'An alternating frequency/time domain method for calculating the steady-state response of nonlinear dynamic systems', *Journal of Applied Mechanics* **56**(1), 149–154.

Dowell, E. (1981), 'Non-linear oscillator models in bluff body aero-elasticity', *Journal of Sound and Vibration* **75**(2), 251–264.

Facchinetti, M., de Langre, E. and Biolley, F. (2004), 'Coupling of structure and wake oscillators in vortex-induced vibrations', *Journal of Fluids and Structures* **19**(2), 123–140.

Jenkins, G. (1962), 'Analysis of the stress-strain relationships in reactor grade graphite', *British Journal of Applied Physics* **13**, 8–10.

Krack, M. (2015), 'Nonlinear modal analysis of nonconservative systems: Extension of the periodic motion concept', *Computers & Structures* **154**, 59–71.

Laxalde, D., Salles, L., Blanc, L. and Thouverez, F. (2008), 'Non-linear modal analysis for bladed disks with friction contact interfaces', *ASME. Paper No. GT2008-50860* .

Laxalde, D. and Thouverez, F. (2009), 'Complex non-linear modal analysis for mechanical systems: Application to turbomachinery bladings with friction interfaces', *Journal of Sound and Vibration* **322**(4), 1009–1025.

Laxalde, D., Thouverez, F. and Lombard, J.-P. (2010), 'Forced response analysis of integrally bladed disks with friction ring dampers', *Journal of Vibration and Acoustics* **132**(1), 011013.

Laxalde, D., Thouverez, F., Sinou, J.-J. and Lombard, J.-P. (2007), 'Qualitative analysis of forced response of blisks with friction ring dampers', *European Journal of Mechanics A/Solids* **26**(4), 676 – 687.

Lupini, A. and Epureanu, B. I. (2020), 'A friction-enhanced tuned ring damper for bladed disks', *Journal of Engineering for Gas Turbines and Power* **143**(1), 011002.

Mead, D. J. (1975), 'Wave propagation and natural modes in periodic systems: I. mono-coupled systems', *Journal of Sound and Vibration* **40**(1), 1–18.

Pešek, L., Půst, L. and Šnábl, P. (2019), Study of dry-friction damping effect on two simplified models of flutter oscillations, *in* T. Uhl, ed., 'Advances in Mechanism and Machine Science', Springer International Publishing, Cham, pp. 3419–3428",.

Půst, L. and Pešek, L. (2017), 'Blades forced vibration under aero-elastic excitation modeled by van der pol', *International Journal of Bifurcation and Chaos* **27**(11), 1750166.

Půst, L., Pešek, L. and Byrtus, M. (2018), 'Modelling of flutter running waves in turbine blades cascade', *Journal of Sound and Vibration* **436**, 286–294.

Rosenberg, R. M. (1960), 'Normal modes of nonlinear dual-mode systems', *Journal of Applied Mechanics* **27**(2), 263–268.

Salles, L. and Vahdati, M. (2016), 'Comparison of two numerical algorithms for computing the effects of mistuning of fan flutter', *ASME. Paper GT2016-57324* .

Sarrouy, E. (2019), Phase driven modal synthesis for forced response evaluation, *in* '7 th International Conference on Nonlinear Vibrations, Localization and Energy Transfer', Marseille, France.

Shaw, S. W. and Pierre, C. (1991), 'Non-linear normal modes and invariant manifolds', *Journal of Sound and Vibration* **150**(1), 170–173.

Stapelfeldt, S. and Brandstetter, C. (2020), 'Non-synchronous vibration in axial compressors: Lock-in mechanism and semi-analytical model', *Journal of Sound and Vibration* **488**, 115649.

Sun, Y., Vizzaccaro, A., Yuan, J. and Salles, L. (2021), 'An extended energy balance method for resonance prediction in forced response of systems with non-conservative nonlinearities using damped nonlinear normal mode', *Nonlinear Dynamics* **103**(4), 3315–3333.

Sun, Y., Yuan, J., Denimal, E. and Salles, L. (2021), 'Nonlinear modal analysis of frictional ring damper for compressor blisk', *Journal of Engineering for Gas Turbines and Power* **143**(3), 031008.

Sun, Y., Yuan, J., Pesaresi, L., Denimal, E. and Salles, L. (2020), 'Parametric study and uncertainty quantification of the nonlinear modal properties of frictional dampers', *Journal of Vibration and Acoustics* **142**(5), 051102.

Sun, Y., Yuan, J., Pesaresi, L. and Salles, L. (2018), 'Nonlinear vibrational analysis for integrally bladed disk using frictional ring damper', *Journal of Physics: Conference Series* **1106**, 012026.

Sun, Y., Yuan, J., Vizzaccaro, A. and Salles, L. (2021), 'Comparison of different methodologies for the computation of damped nonlinear normal modes and resonance prediction of systems with non-conservative nonlinearities', *Nonlinear Dynamics* **104**, 3077–3107.

Tang, W. and Epureanu, B. I. (2019), 'Geometric optimization of dry friction ring dampers', *International Journal of Non-Linear Mechanics* **109**, 40 – 49.

Urabe, M. (1965), 'Galerkin's procedure for nonlinear periodic systems', *Archive for Rational Mechanics and Analysis* **20**(2), 120–152.

Vahdati, M., Simpson, G. and Imregun, M. (2011), 'Mechanisms for wide-chord fan blade flutter', *Journal of Turbomachinery* **133**(4), 041029.

Wu, Y., Li, L., Fan, Y., Zucca, S., Gastaldi, C. and Ma, H. (2020), 'Design of dry friction and piezoelectric hybrid ring dampers for integrally bladed disks based on complex nonlinear modes', *Computers & Structures* **233**, 106237.

Zhao, F., Smith, N. and Vahdati, M. (2017), 'A simple model for identifying the flutter bite of fan blades', *Journal of Turbomachinery* **139**(7), 071003.